IL NUOVO CIMENTO Vol. 37 C, N. 4 Luglio-Agosto 2014
DOI 10.1393/ncc/i2014-11787-1

Communications: SIF Congress 2013

Simulation of low-energy antiproton annihilation in silicon

A. Magnani

INFN, Sezione di Pavia and Dipartimento di Fisica, Università di Pavia - Pavia, Italy

ricevuto il 31 Gennaio 2014; approvato il 19 Maggio 2014

Summary. — The simulation of the interaction of low-energy antiprotons in a silicon target is of primary importance to the AEGIS Collaboration at CERN. In Geant4 two different models, called CHIPS and FTFP, are implemented for the simulation of $\bar{p}$-nucleus annihilation at rest, but their validation is currently incomplete. The study presented in the following aims at describing their behavior while dealing with annihilation at rest in silicon, comparing their results on the one hand with data available in the literature and on the other hand with data collected by the AEGIS Collaboration using a silicon prototype.

PACS 24.10.Lx – Monte Carlo simulations (including hadron and parton cascades and string breaking models).
PACS 25.43.+t – Antiproton-induced reactions.

1. – The AEGIS experiment

AEGIS (Antihydrogen Experiment: Gravity, Interferometry, Spectroscopy) is one of the experiments currently in operation at the Antiproton Decelerator (AD) facility at CERN and dealing with antihydrogen physics.

Since the production of the first antihydrogen atoms accomplished in 1995 at the Low Energy Antiproton Ring (LEAR) [1], this research field has been receiving more and more interest in CERN community, and now it plays a primary role in the CERN research program, alongside the high-energy particle physics which the Large Hadron Collider stands for.

The birth of AD [2], which replaced LEAR in 1997, paved the way for two successful experiments, called ATHENA [3] and ATRAP [4]. These collaborations developed experimental techniques which allowed the production of considerable amounts of antihydrogen having low kinetic energy, so that the first measurements of antihydrogen properties became possible [5, 6].

The know-how acquired by these experiments in handling antimatter is now an invaluable heritage for ASACUSA [7], ALPHA [8] and AEGIS [9], the other collaborations

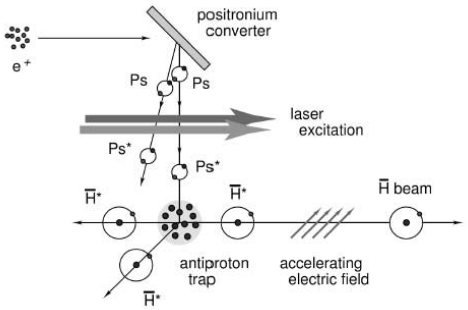

Fig. 1. – The main steps leading to the antihydrogen beam in the AEGIS experiment.

hosted by the AD with the purpose of exploiting ultra-cold antihydrogen as a test-bench to probe fundamental physical principles.

In particular, the AEGIS experiment aims at measuring the Earth gravitational acceleration g on antihydrogen atoms. In the first phase of the experiment, the collaboration expects to obtain a value of g with 1% precision. The physical significance of such result would be remarkable, as it would be the first direct measurement of the gravitational acceleration of antimatter ever performed so far, apart from the very preliminary study published by the Alpha Collaboration [10]. Besides the experimental importance of such a measurement without precedent, it must be stressed that the consequences of the result could give a notable contribution to a fascinating research field, including modern quantum gravity theories and the searches for violations of the weak equivalence principle.

The g measurement will be carried out by sending an antihydrogen beam through a classical moiré deflectometer coupled to a position sensitive detector. The main steps of the experiments are summed up in fig. 1. The antihydrogen atoms will be produced

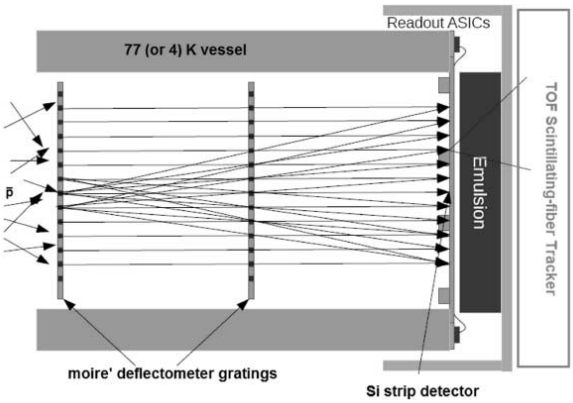

Fig. 2. – Sketch of the moiré deflectometer and of the position-sensitive detector, whose design is currently in course [11].

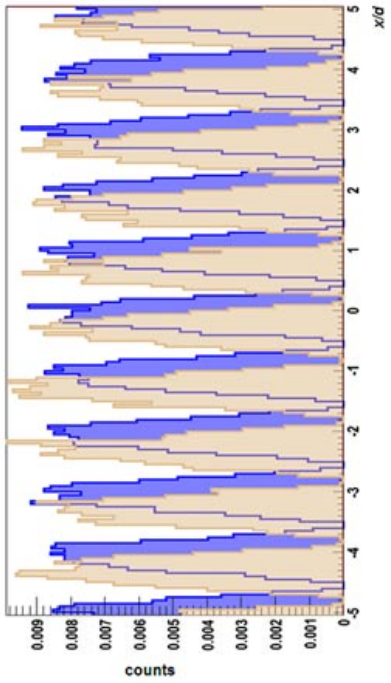

Fig. 3. – Typical moiré pattern obtained in a Monte Carlo simulation with (light fringes) and without (dark fringes) gravitational force.

through the charge-exchange reaction:

$$Ps^* + \bar{p} \longrightarrow \bar{H}^* + e^-,$$

where Ps stands for positronium and the "*" stands for a Rydberg state. The sensitivity of Rydberg atoms to electric field gradients will be exploited to form an antihydrogen beam through the so-called "Stark acceleration": a suitable non-uniform electric field will give the atoms a velocity boost of a few hundreds m/s in the longitudinal direction towards the deflectometer. Such a device, shown in fig. 2, is made of two gratings with a pitch of the order of $40\,\mu$m. The antiatoms which will have managed to pass through the slits will impinge upon a position sensitive detector, serving the purpose of measuring the vertical position and the arrival time of each antihydrogen atom. Due to the projection of the deflectometer's shadow on the detector's surface, the annihilation signals will be distributed in a fringe pattern, similar to the one shown in fig. 3. The gravitational force acting on the beam will make this figure slide vertically downwards of a length:

$$\delta x = -gT^2,$$

where T is the antihydrogen time of flight between the two gratings. T can be determined thanks to an experimental measurement of the difference between the Stark acceleration time and the annihilation time. Therefore, measuring δx, the value of g can be extracted.

The uncertainty on the gravitational acceleration is dominated by the performance of the position-sensitive detector in the reconstruction of the antihydrogen impact point. In order to achieve the desired accuracy, the device should cover approximately a $10 \times 10\,\mathrm{cm}^2$ wide surface and must be able to measure the arrival time of the antiatoms with resolution of some μs and their vertical coordinate with a resolution of about 10–13 μm.

According to the current design, a hybrid detector will be implemented. It will include a 50 μm thick silicon strip detector, followed by an emulsion part expected to reach a spatial resolution of 1–2 μm [12, 13] and a scintillating fiber tracker. Since the antihydrogen beam will have a longitudinal velocity of a few hundreds m/s, corresponding to a kinetic energy of only few meV, the antiatoms reaching the device will be immediately stopped in the first atomic layers of the silicon detector, where they will annihilate at rest.

Since electron-positron annihilation only results in the emission of γ-rays, the process responsible for the signal in the hybrid detector is antiproton annihilation on ^{28}Si nuclei. An accurate simulation of such a process is of crucial importance to the experiment. Not only Monte Carlo simulations studying the detector's response to antiproton annihilation are expected to provide the desired guidelines in view of its design, but the very procedure leading to the measurement of g is based on the comparison between the experimental moiré pattern formed on the detector by antiatoms flying in the Earth's gravitational field with the one resulting from a simulation not including the gravitational force.

2. – Geant4 antiproton-nucleus annihilation models

At the moment, Geant4 includes different models dealing with antiproton-nucleus annihilation, but their validation is still an open issue, due to the lack of experimental data concerning annihilation at rest on silicon. This makes choosing the physics parameters to be used in the AEGIS Monte Carlo as hard as decisive.

In the Geant4 context, the models devised to predict the final state of a generic interaction can be distinguished in three basic types: models that are predominantly based on experimental data, models that are predominantly based on parameterizations and extrapolation of experimental data under some theoretical assumptions, and models that are predominantly based on theory [14]. When sufficient coverage is available for the experimental data, the data driven approach is considered the optimal and safest way of modelling. However, this is not possible in the case of annihilation at rest.

In contrast, Geant4 offers two theory driven models, called CHIPS (Chiral Invariant Phase Space) and FTFP (FriTioF plus Precompound). In addition to them, also the Low Energy Parameterised model LEP is present. The parameterized models come from the translation into Geant4 of Geant3 codes, especially the hadronic intarection package named Geisha. The performance of LEP is widely considered less accurate than the alternative models cited above, so that it won't be taken into account in this discussion.

The CHIPS [15] event generator was implemented in Geant4 to simulate a wide range of hadron and lepton nuclear processes, though its main strength is the nuclear capture at rest of negatively charged hadrons (π^-, k^-, $\bar{p}$, Σ^-, $\bar{\Sigma}^+$, Ξ^-, Ω^-). For a long time it had been considered the most promising tool for antinucleon annihilation modelling, and was expected to find application in most of the AD experiments.

As for p-$\bar{p}$ annihilation at rest, CHIPS behavior has been extensively validated also thanks to experimental data collected by the Crystal Barrel experiment, where antiprotons slowed down by LEAR were stopped in liquid hydrogen [16].

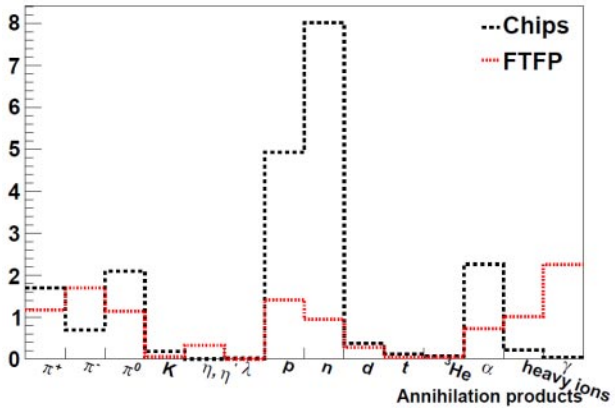

Fig. 4. – Distribution of annihilation prongs with CHIPS and FTFP [11].

As far as $\bar{p}$-nucleus annihilation at rest is concerned, official validations are available only for carbon and uranium. They show a reasonable agreement with experimental data, although some inconsistency can be found mainly in proton and pion spectra. Details about the outcome of the validation can be found in [17].

A serious issue related to the CHIPS generator consists in the complexity of its code, which makes it difficult to keep it up-to-date with the more and more recent versions of Geant4, so that the Geant4 hadronic group has planned its gradual replacement with alternatives models. The model has been definitely dismissed starting from the Geant4.10 release.

On the other hand, FTFP [18] is a novel code that provides nuclear interactions of antibaryons ($\bar{n}$, $\bar{p}$, $\bar{\Lambda}^0$, $\bar{\Sigma}^+$ $\bar{\Sigma}^-$, $\bar{\Sigma}^0$, $\bar{\Xi}^+$, $\bar{\Xi}^0$, $\bar{\Omega}^-$) for energies ranging from 0 up to the order of TeV and it could offer a good alternative description of $\bar{p}$-nucleus annihilation.

Its name refers to an integration of the Precompound de-excitation model [19] in the frame of the Fritiof string model (FTF) [20]. It has been so far validated only for annihilation in flight, using data obtained with antiprotons having kinetic energy of a few hundred MeV [18].

3. – Comparison between Geant4 and the LEAR data

Figure 4 shows the distribution of annihilation prongs produced in a Geant4 simulation where 2 meV antiprotons impinge perpendicularly upon the surface of a sensitive silicon layer. This histogram highlights the different structure of the annihilation event in the two generators. In CHIPS the involved ^{28}Si nucleus breaks up in many light nuclear fragments, especially protons, neutrons and alphas, while heavier fragments are produced only in the 20% of the events. The features of the FTFP model, instead, are typical of an annihilation taking place at the nuclear periphery. As a matter of fact, a heavy residual nucleus, such as Al, Mg or O, is always sent out, together with a few spare nucleons coming from the residual nucleus de-excitation through a nucleon evaporation process.

Although data concerning annihilation at rest in silicon are not available in literature, it's interesting to compare the results of this simulation with the experimental information collected at LEAR for other nuclei.

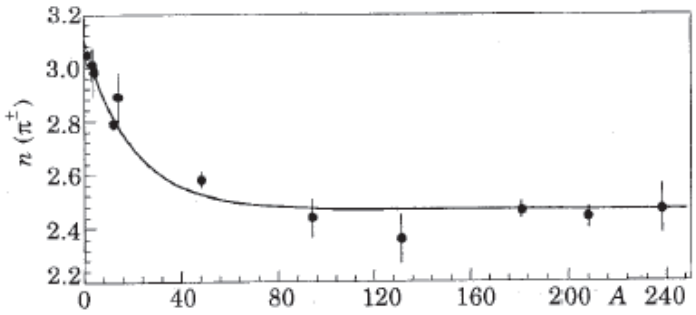

Fig. 5. – Experimental mean charged pion multiplicity $n_{\pi^\pm}$ for antiproton annihilation at rest on different nuclei as a function of the mass number A. The line is the result of a best-fit calculation [21].

First of all, it can be noted that in FTFP negative pions are produced more frequently than positive ones, in contrast to CHIPS. This is in agreement with data, where the yield of negative pions is greater with respect to positive ones in antiproton-nucleus annihilation, due to charge conservation [21].

In addition to that, the overall charged pion multiplicity $n_{\pi^\pm}$ obtained as a function of the mass number A of the target nucleus is shown in fig. 5. Starting From $A = 2$, $n_{\pi^\pm}$ decreases quickly as A increases for $A < 80$ and is almost constant above. According to this plot a value of $n_{\pi^\pm}$ roughly ranging from 2.5 and 2.8 can be expected for annihilation in silicon. The simulation provides an overall charged pion yield $n_{\pi^\pm}$ of about 2.3 and 2.8 pions per annihilation for CHIPS and FTFP respectively, so that the FTFP result seems more consistent with experimental data.

As for the nuclear part of the annihilation products, one of the LEAR experiments investigated the yield of light nuclear fragments in annihilation at rest on different targets [22]. Although silicon is not included, a behaviour roughly intermediate between the ones of ^{12}C and ^{40}Ca might be expected. The experimental yields are shown in table I, together with the simulation results. This comparison has been already shown in [11]. The listed numbers include only nuclear fragments having kinetic energy within the sensitivity range of the experiment, which is reported in the first column. Since this energy window is very narrow, the study is not sufficient to investigate the reliability of the

TABLE I. – *Measured and simulated production yield (for* 100 *annihilations) of different nuclear fragments in the energy range given by the first column and produced in antiproton annihilation at rest on different nuclei. Experimental data coming from LEAR for* ^{12}C *and* ^{40}Ca *are compared to simulation obtained with CHIPS and FTFP for* ^{12}C*, and* ^{40}Ca *and* ^{28}Si [11].

	Energy (MeV)	LEAR ^{12}C	CHIPS ^{12}C	FTFP ^{12}C	CHIPS ^{28}Si	FTFP ^{28}Si	CHIPS ^{40}Ca	FTFP ^{40}Ca	LEAR ^{40}Ca
p	6-18	23±2	168±1	56.0±0.8	170±1	58.6±0.8	172±1	60.2±0.8	74±4
d	8-24	9.3±0.8	15.9±0.4	12.1±0.3	15.9±0.4	12.2±0.3	14.9±0.4	12.0±0.3	18±1
t	11-29	4.5±0.4	2.8±0.2	1.3±0.1	3.0±0.2	1.5±0.1	2.7±0.2	1.0±0.1	5.7±0.4
^{3}He	36-70	1.7±0.2	0.19±0.01	0.11±0.03	0.23±0.05	0.16±0.04	0.22±0.05	0.13±0.04	2.2±0.2
α	36-70	1.1±0.1	1.8±0.1	0	1.8±0.1	0	1.9±0.1	0	2.2±0.2

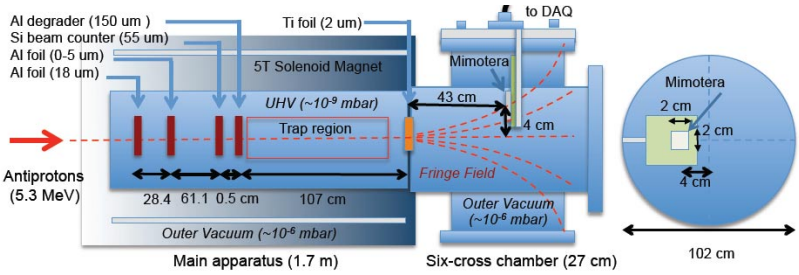

Fig. 6. – Top view (left) and axial view (right) of the setup. The center of the MIMOTERA is installed 40 mm off-axis and 430 mm from the main apparatus to avoid saturation due to the high beam intensity [11].

models. In spite of that, it shows an overall compatibility with experimental data, apart from a clear excess in the number of protons delivered by CHIPS and an underestimation of α-particles in FTFP.

In conclusion, as far as information coming from LEAR is concerned, the FTFP model offers the great advantage of a satisfying pion multiplicity, in contrast to CHIPS. Also the production of protons gives some hints in favour of FTFP. On the other hand, CHIPS seems to reproduce better the yields of the other light nuclear fragments, in particular α-particles.

4. – Comparison between Geant4 and the MIMOTERA data

During the AD run in June 2012, a silicon detector called MIMOTERA [23] was exposed to the AEGIS antiproton beam-line, in order to collect the first data concerning antiproton annihilation at rest in silicon. In the present section, the results are compared to Geant4 simulation, using CHIPS and FTFP.

MIMOTERA is a monolithic active pixel sensor using CMOS technology. Its surface is $2 \times 2\,\mathrm{cm}^2$ wide and it is divided into 112×112 pixels, each one covering $153 \times 153\,\mu\mathrm{m}^2$. The active silicon layer is $14\,\mu$m thick and it is mounted on $600\,\mu$m thick silicon support. Details about the detector, the experimental procedure for data-taking and the data analysis can be found in [11].

The detector was mounted downwards the 5 Tesla magnet hosting the AEGIS antiproton beamline. Antiprotons were delivered by the AD in 120 ns long bunches containing 3×10^7 particles each, with kinetic energy of 5.3 MeV. Entering the bore inside the AEGIS magnet, they slowed down going through various degraders, arriving at the surface of the MIMOTERA with a kinetic energy af a few hundreds keV. A view of the experimental setup is sketched in fig. 6. The AEGIS beam line was entirely reproduced in the simulation.

Each AD spill resulted in a number of clusters on the surface of the detector. The parameters of such clusters have been taken into account to carry out a comparison between data and simulation. In particular, four different distributions which could highlight the differences between CHIPS and FTFP have been examined, in order to understand which model offers the best description of experimental data:

– the cluster multiplicity distribution (n_{pix});

– the distribution of the highest energy deposited in a single pixel (E_1);

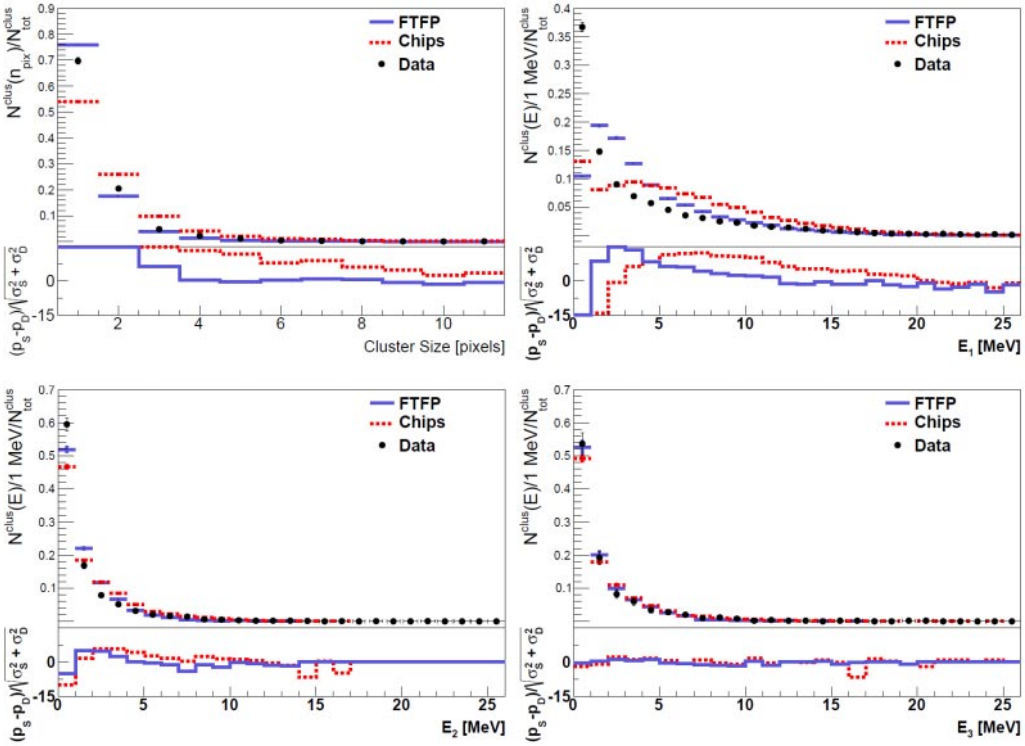

Fig. 7. – From top left, clockwise: cluster multiplicity distribution; E_1 distribution; E_2 distribution; E_3 distribution. All histograms are normalized to 1. Below each histogram the deviation of the simulated points with respect to experimental ones $((p_S - p_D)/\sqrt{\sigma_S^2 + \sigma_D^2})$ is plotted both for CHIPS and FTFP.

– the distribution of the second highest energy deposited in a single pixel (E_2);

– the distribution of the energy deposited in the cluster, excluding the first two pixels with the highest energy ($E_3 = E - E_1 - E_2$, being E the energy deposited in the entire cluster).

Such distributions are reported in fig. 7. While the experimental E_3 distribution is correctly reproduced by both generators, E_1 and E_2 show a poor agreement with simulation in the low-energy region. Above a few MeV, FTFP seems to be the best model. Also for the cluster multiplicity, FTFP is closer to data than CHIPS.

Moreover, variables which could be less sensitive to possible sources of systematic errors on the energy deposited in the detector have been considered:

– the E_1/E ratio;

– the E_2/E ratio;

– the $(E - E_1 - E_2)/E = E_3/E$ ratio.

In order to verify the stability of the analysis, a scan of the mean value of these distributions has been performed as a function of the energy threshold applied on single pixels

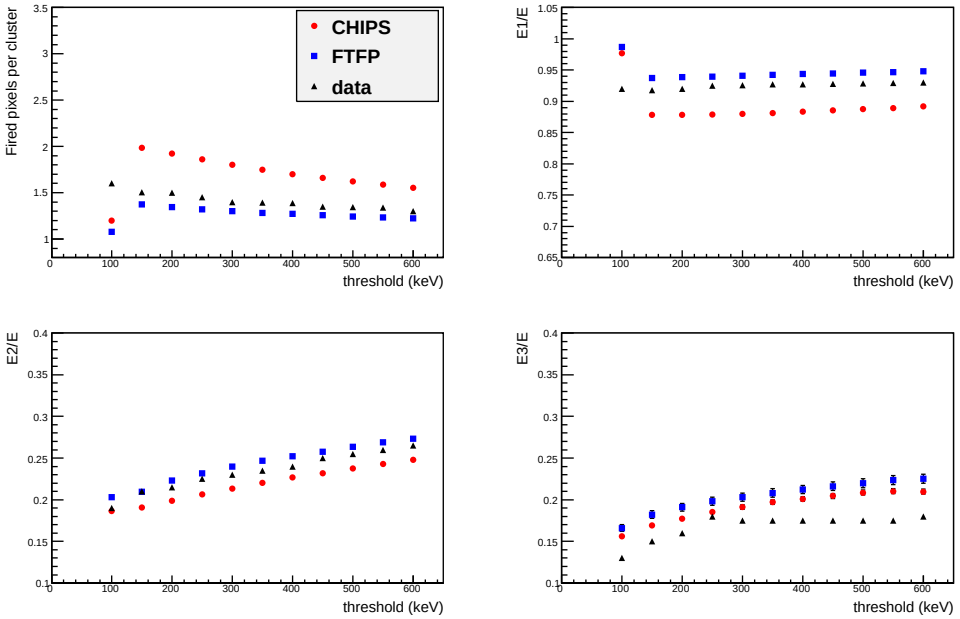

Fig. 8. – From top left, clockwise: scan of the mean value of n_{pix}, E_1/E, E_2/E and E_3/E as a function of the energy cut on single pixels. The errorbars are smaller than the points' size.

(both in data and in the simulation) to cut off the electronic noise. Such a threshold was moved in the range from 100 keV to 600 keV. Results are shown in fig. 8. The scan exhibits a reasonable agreement between data and simulation for n_{pix}, E_1/E and E_2/E, that favors FTFP model. The comparison gives poorer results for the E_3/E distribution.

5. – Conclusion

The analysis carried out with the MIMOTERA detector has revealed the Geant4 models CHIPS and FTFP are not always statistically compatible with experimental results. In spite of that, they provide a roughly reasonable description of data, which is an acceptable result for two theory driven models. In particular, FTFP predictions have been found closer to experimental data than CHIPS.

The work described here is related to the first study about antiproton annihilation at rest in silicon; the tests performed on the Geant4 models will pave the way to the Monte Carlo simulations for the detector design and to the data analysis of the AEGIS experiment.

* * *

I would like to thank the AEGIS Collaboration, Alberto Ribon of the Geant4 hadronic group for his help and assistance, the Bergen Research Foundation and the Research Council of Norway for providing financial support.

REFERENCES

[1] Baur G. *et al.*, *Phys. Lett. B*, **368** (1996) 251.
[2] Landua R., *Phys. Rep.*, **403-404** (2004) 323.
[3] Amoretti M. *et al.*, *Nucl. Instrum. Methods A*, **518** (2004) 679.
[4] Gabrielse G. *et al.*, *Phys. Rev. Lett.*, **89** (2002) 233401.
[5] Amoretti M. *et al.*, *Nature*, **419** (2002) 456.
[6] Tan J. N. *et al.*, *Nucl. Instrum. Methods B*, **214** (2004) 22.
[7] Enomoto Y. *et al.*, *Phys. Rev. Lett.*, **105** (2010) 243401.
[8] Andersen G. B. *et al.*, *Nature*, **468** (2010) 673.
[9] The AEGIS Collaboration, CERN-SPSC-2007-017 (2007).
[10] Charman A. E. (The ALPHA Collaboration), *Nat. Commun.*, **4** (2012) 1785.
[11] Aghion S. *et al.*, *JINST*, **9** (2014) P06020.
[12] Amsler C. *et al.*, *JINST*, **8** (2013) P02015.
[13] Aghion S. *et al.*, *JINST*, **8** (2013) P08013.
[14] Wellisch J. P., arXiv:nucl-th/0306006v1 (2003).
[15] Degtyarenko P. V. *et al.*, *Eur. Phys. J. A*, **8** (2000) 217.
[16] Amsler C., *Rev. Mod. Phys.*, **70** (1998) 1293.
[17] Kossov M., *IEEE Trans. Nucl. Sci.*, **52** (2005) 2832.
[18] Galoyan A. and Uzhinsky V., arXiv:1208.3614v1 [hep-ph] (2012).
[19] Geant4 Physics Reference Manual, `http://geant4.cern.ch/support/userdocuments.html`.
[20] Andersson B. *et al.*, *Nucl. Phys. B*, **281** (1987) 289.
[21] Bendiscioli G. and Kharzeev D., *Riv. Nuovo Cimento*, **17** No. 6 (1994) 1.
[22] Markiel M. *et al.*, *Nucl. Phys. A*, **485** (1988) 445.
[23] Boll R. *et al.*, *Radiat. Meas.*, **46** (2011) 1971.